# Role of the electrolyte in gas formation during the cycling of a Gr//NMC battery as a function of temperature: Solvent, salt, and ionic liquid effect.

Mohamed Raghibi, Baokou Xiong, Satyajit Phadke, Mérièm Anouti

# Role of the electrolyte in gas formation during the cycling of a Gr//NMC battery as a function of temperature: Solvent, salt, and ionic liquid effect.

*Mohamed Raghibi[a], Baokou Xiong[a], Satyajit Phadke[a], and Mérièm Anouti[a]**

[a] *Laboratoire PCM2E, Université de Tours, Parc de Grandmont, 37200, Tours, France*

Corresponding author: meriem.anouti@univ-tours.fr

**Abstract**

The operation of lithium-ion batteries, whether normal or in abusive conditions, is accompanied by the generation of gas in particular during the first cycles. This is intrinsic to the device and is subject to numerous parameters such as the electrode materials used, the electrolyte or even the operating conditions. This generation of gas is harmful: it leads to an increase in the internal pressure of the batteries, raising safety problems. In the present study we propose an original experimental protocol to measure the volume of gas generated during cycling of Gr//NMC full cell in pouch cells systems. We compared the values obtained at two temperatures with 7 different electrolytes formulated with 4 alkylcarbonate solvents (EC, PC, DMC, EMC), two salts ($LiPF_6$ and LiTFSI) and 2 ionic liquids, methyl butyl pyrrolidinium bis (trifluoro-sulfonyl) imide ($Pyrr_{14}$ TFSI) and methyl tributyl phosphonium bis (trifluoro-sulfonyl) imide ($Phos_{1444}$ TFSI). The gases generated were identified by GC/MS and the gas solubility ($O_2$, $H_2$) was measured ex-situ. The objective was to discern the respective roles of salts, solvents and ionic liquids on the swelling of the batteries. The results showed that the quantity of gas produced is essentially linked to the formation of the solid electrolyte interphase (SEI) at the first charge. It is greater in the case of LiTFSI compared to $LiPF_6$ (2.8 mL vs 1.9 mL). The quantities of gas were correlated with the solubility of gases in the electrolyte measured for $H_2$ and $O_2$ with and without salt. The LiTFSI result allows a "salting in" effect which physically results in the wilting of the pouch cells and a reduction in the volume of gas during cycling. This phenomenon, attributed to a better solubility of the gases produced in the electrolyte in the presence of this salt, is accentuated with temperature. Lastly, analysis of the gas composition by GC-MS revealed a predominance of $CO_2$ and $CH_4$ gases and confirmed the effect of salt in the quantity and composition of the gas mixture. Ionic liquids and LiTFSI are interesting at high temperatures and for systems subject to high gas generation especially $O_2$, such as transition metal oxide cathodes.

**Keywords**: Electrolyte, Lithium-ion, batteries, gas volume, pouch cell swelling, safety

## 1. Introduction

The generation and management of gases in Li-ion batteries is drawing the attention of both industrialists [1, 2] and the research community in this field [3, 4]. The objective is to identify and quantify the gases to understand the origin of their formation and to remedy the harmful consequences of their accumulation during battery operation [5]. Gas generation is a complex phenomenon depending on various parameters such as the composition of the electrolyte, the nature of the electrodes, the cycling regime or even operating conditions such as temperature and the cutoff voltage [1, 6, 7]. It can therefore be difficult to find the ideal conditions to minimize the amount of gas generated and its effect on aging and safety. Consequently, this problem cannot be overlooked because, beyond optimizing battery performance, safety is a particularly sensitive aspect for consumer use of batteries [8-10]. The generation of gases in lithium-ion batteries poses above all a technological challenge [11, 12]. Their accumulation in sealed batteries prevents their evacuation, which increases the danger. The generation and evolution of gases during battery operation and storage, that is to say without electrochemical cycling, significantly reduces the battery lifespan and cyclability [9, 13].

The majority of the reactions that produce gases in accumulators are localized at the electrode / electrolyte interfaces, which are particularly sensitive areas [10]. The gases create vacuum zones which cause a displacement of the electrolyte to fill this vacuum, causing a discontinuity in the diffusion of the species in solution, in particular the lithium ions. In general, the phenomena of gas generation and their accumulation at the interfaces result in an increase in the electrical resistance of the cell [14], but also in an increase in internal pressure, leading to mechanical stress of the electrode materials. Swelling ranging from 6 to 20% is observed on average after storage at high temperature for commercial pouch cells [15]. In addition, other intrinsic aging parameters of the batteries due to the cycles of intercalation / deintercalation of lithium ions further reduce the lifespan of the battery.

For all these reasons, it is important to identify the electrolyte components that promote the generation of gas in lithium-ion batteries and those that on the contrary reduce it. The accumulation of gases in cells cannot be dissociated from their solubility in electrolytes. Gas solubility measurements have already been reported in the literature [16, 17] and by our group [18-21] which has reported data concerning the ex situ measurement of solubility as a function of the composition of the electrolyte and the temperature. However, the solubility of gas alone is not sufficient to understand the overpressure mechanisms in lithium-ion batteries because these measurements do not take into account real conditions during cycling,

including the catalytic activity of the charged electrode material interfaces. Few studies have quantified the volume of gas generated and its correlation to operating conditions and the electrolyte composition. Dahn et al., for example, focused on these measures through the study of the effect of additives on gas generation [22, 23]. They reported pressure measurements in the presence of additives such as flame retardants (TTFP, TTSPi)[24], or polymerization initiators [25, 26]. The paucity of data on the quantification of gases generated during cycling no doubt resides in the difficulty in implementing these measures without disturbing cell cycling. In the present study, we report the development of an original protocol allowing the measurement of the volume of gas generated during cycling of Gr//NMC in pouch-cell systems. We compare the values obtained at two temperatures with different electrolyte formulations. The identification of the gases generated by GC/MS as well as ex-situ measurement of the gas solubility ($O_2$, $H_2$) carried out in this study made it possible to discuss the results obtained. The aim was to discern the respective roles of salts, solvents and two ionic liquids at two concentrations (5% and 30% wt) to understand their impact on battery swelling.

## 2. Methodology and procedure

### 2.1. Pouch cell preparation and gas volume measurements

The Gr//NMC pouch cells used in this study were purchased empty, to be filled with electrolyte, from the company Li-Fun corporation (China) and sealed under vacuum. They can deliver a capacity of 200 mAh for a cutoff voltage of 4.2 V. The positive electrode dimensions are 200 mm x 26 mm while the negative electrode measures 204 mm x 28 mm. The two electrodes are coated on both sides; a free strip at the end of the roll allows sealing without the risk of short circuit. The size of the active surface is between 90 and 100 cm². The electrodes are wound with a Celgard type separator. Before filling them with electrolyte, the pouch cells, initially sealed under vacuum without electrolyte, are opened and dried under vacuum at 80 ° C for 12 hours to remove traces of water. The cells are then transferred to a glove box to be filled with the electrolyte without contamination. The bags are sized for 0.9 g (approximately 1 mL) of electrolyte (supplier recommendation).

The sealing of the filled pouch cells is carried out using a vacuum heat sealer with controlled pressure and temperature. To improve the wettability of the electrodes and the separator, the pouch cells are charged at 1.5 V v.s $Li^+/Li$ and maintained at this voltage for 24 hours at room temperature in order to polarize the electrodes without initiating intercalation processes.

The volume measurement of the pouch cells was carried out before the first cycle, (to determine the volume of the pouch cells before gas generation), and after each end of charging and discharging. This means that two volume measurements were made per cycle. The volume of the pouch cell was determined by means of two successive weighings using a device (**Figure 1a**) adapted to the precision balance from Sertorius. The first weighing was carried out with the basket (**Figure 1b**) placed on the support (in the air), and the second was performed with the basket plunged into distilled water. The volume of the pouch cell according to their swelling state (**Figures 1 c and d**) is then calculated using the following equation:

$$V_{\text{pouch cell}} = \frac{m_{air} - m_{water}}{\rho_{water}} \text{ with } \Delta V = \pm 10^{-2}\text{mL}$$

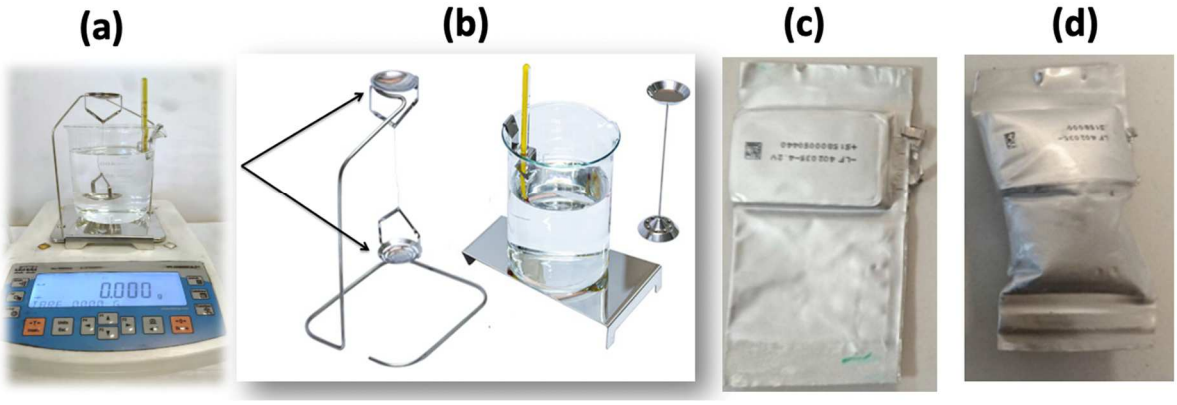


**Figure 1.** Device for measuring pouch cell volume (a), weighing basket (b), Photos showing two pouch cells according to their swelling state (c, d).

The repeatability of the measurements was ensured by the meticulous preparation of the pouch cells in an opening, drying, filling and then sealing process to avoid problems of electrolyte and / or gas leakage due to poor sealing. To prevent the released gases from being inserted at the jelly-roll level (**Figure 2a**), which leads to an increase in the cell resistance by separation of the battery elements (electrodes, separator), we pressed the pouch cells as shown in (**Figure 2c**). Four pouch cells were pressed at 2 $N.m^{-1}$ using a torque wrench (**Figure 2b**) and tested simultaneously to ensure the reliability of the measurements. The applied pressure maintains sufficient optimum stress for the cohesion of the battery without causing the pouch cells to open at the jelly-roll level and therefore the leakage of the electrolyte or the gases.

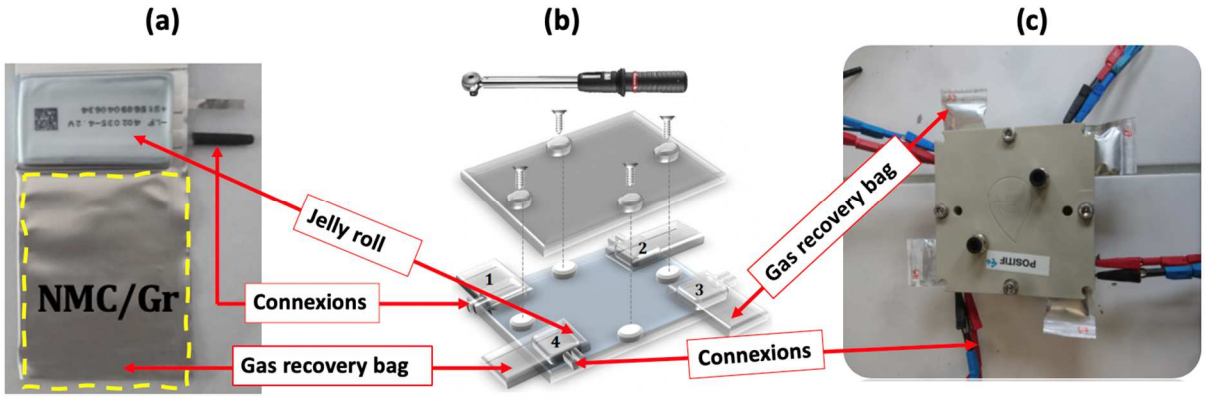


**Figure 2**. Different elements of a pouch cell (a), Torque wrench and pressing system (b), photo of a 4 pouch cells system pressed between two plates at a pressure of $2N.m^{-1}$ (c)

2.2. Repeatability and uncertainty

The electrochemical and volume measurements showed good repeatability both for galvanostatic profiles and for gas volumes. **Figure 3** shows the galvanostatic profiles of the first cycle obtained during reproducibility tests on four different pouch cells (**Figure 3a**), and the repetition of five volume measurements for each of them (**Figure 3b**). The pouch cell characterization methodology was validated for the rest of this work with a volume measurement error between 2% and 4%.

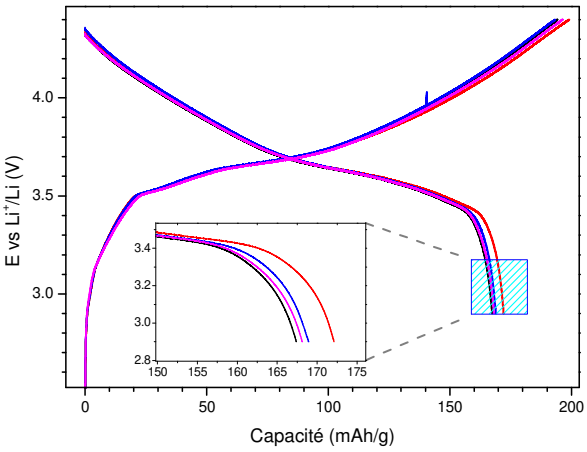


**Figure 3.** Comparison of galvanostatic profiles obtained for the first cycle in the case of four different Gr // NMC pouch cells (a) and repeatability of volume measurements (b).

2.3. Gas analysis

The composition of the gases in the pouch cells was analyzed by gas chromatography coupled with mass spectroscopy (GC-MS) in order to detect the gases described as mainly responsible for battery swelling, i.e. $CO_2$, CO, $CH_4$, $C_2H_4$, $H_2$, and O2. The gas mixture was

taken directly from the pouch cells at the end of the cycle using a "gas-tight" type chromatography syringe, and the collected gas mixture was injected directly into the column. The oven was maintained at 50 ° C for a carrier gas flow rate set at 0.5 mL.min-1. The optimal volume for detection was 2 µL to analyze even slightly swollen pouch cells.

2.4. Electrolyte vapor pressure and gas solubility

The measurement of gas solubility was carried out by bringing a known quantity of gas into contact with a quantity of degassed liquid of measured volume and density. The quantity of solubilized gas was obtained by the difference between the initial pressure before addition of gas and the final pressure after thermodynamic equilibrium. The measurement takes into account the free volume occupied by the vapor phase of the solution. The pressure was measured with an accuracy of 0.0 1mBar. The experimental device described by Dougassa *et al.* [18, 20, 21] allows both vapor pressure and gas solubility measurements. In order to ensure repeatability of the results, the experiments were carried out in two identical devices in parallel. The device has a double wall to circulate a thermostatically controlled bath to control the temperature. The electrolyte is introduced in a glove box and is then degassed several times by repeated crystallization cycles under vacuum. When the thermodynamic equilibrium is established, at T given, the vapor pressure of the electrolyte is read.

As the determination of the solubility of gas in the electrolyte is detailed in one of our previous studies [18, 20, 21], we will just summarize it here. The quantity of gas dissolved in the liquid phase is calculated from 2 successive pVT (pressure volume temperature) measurements. During the first pVT measurement, only the electrolyte is present. The device is kept at constant temperature $T_{ini}$, then a quantity of gas is introduced into the equilibrium cell containing the electrolyte. The solubility of the gases in the studied mixture can be expressed as a fraction of their molar fractions in solution, $x_1$: $x_1 = \frac{n_1^{liq}}{n_{solv}^{liq} + n_1^{liq}}$, where $n_1^{liq}$ is the amount of gas dissolved in the liquid solution and $n_{solv}^{liq} = n_2^{liq} + n_3^{liq}$ is the amount of solvent in the liquid phase introduced into the cell. $n_2^{liq}$ corresponds to the quantity of alkyl carbonate solvents, and $n_3^{liq}$ to the quantity of lithium salt in solution. The Henry constant can then be calculated from the molar fraction of solubilized gas according to the equation:

$K_H \equiv \lim_{x_2 \to 0} \frac{f_2(p,T,x_2)}{x_2} \cong \frac{\phi_2(p_{eq},T_{eq})p_{eq}}{x_2}$, where $f_1$ is the fugacity of the gas, and $\varphi_1$ is its coefficient of fugacity at the equilibrium pressure $p_{eq}$ and equilibrium temperature $T_{eq}$.

## 3. Experimental section

### *3.1. Electrolyte formulation*

The electrolyte components were battery-grade ethylene carbonate, EC, (Sigma-Aldrich), ethyl methyl carbonate, EMC, (Sigma Aldrich, 99.9), dimethyl carbonate, DMC, (Sigma Aldrich, 99.9) and propylene carbonate, PC, (Sigma Aldrich, 99.9). The ionic liquids Methyl butyl pyrrolidinium bis (trifluoro-sulfonyl) imide, ($Pyrr_{14}$ TFSI), (Sigma Aldrich, 99), and Methyl tributyl-phosphonium bis (trifluoro-sulfonyl) imide, ($Phos_{1444}$ TFSI), (MTI, 99), were used without prior treatment. For the electrolyte, a binary solvent mixture with a mass ratio of 3/7 or 1/1, and a ternary solvent mixture with a mass ratio of 1/1/3 were formulated in the glove box and mixed with 1.0 mol.$L^{-1}$ of lithium hexafluorophosphate ($LiPF_6$) salt (Sigma Aldrich, battery grade) or 1.0 mol.$L^{-1}$ of lithium bis (trifluoro-sulfonyl) imide (LiTFSI) salt (Sigma Aldrich, 99.95%). The electrolytes were prepared using a Sartorius 1602 MP balance with $\pm 10^{-4}$ g accuracy inside an argon filled MBraun glovebox, at 25 °C, with less than 10 ppm of moisture content. The water content of each electrolyte was measured using an 831 Karl-Fisher Coulometer (Metrohm), with values lower than 20 ppm.

### *3.2. Electrochemical Testing*

The N/P ratio of the Gr//NMC pouch cells with a nominal capacity of 200 mAh for a cutoff voltage of 4.2 V was between 1.1 and 1.4. This ratio corresponds to the ratio of the total anode capacity to the total cathode capacity. The pouch cells were dried under vacuum at 80°C for 12 h and placed in the glovebox without exposure to ambient air. For electrochemical testing, the pouch cells were filled with 1 mL of electrolyte (carefully measured with a micropipette). All the steps involving the pouch cell preparation were performed inside an atmosphere-controlled glovebox where the $H_2O$ and $O_2$ concentration was maintained below 0.1 ppm. Potential limits of 4.2 V – 2.9 V were used for all galvanostatic testing. Galvanostatic cycling was carried out using a VMP multichannel potentiostatic galvanostatic system (Biologic Science Instrument, France).

## 4. Results and Discussion

The electrolyte components chosen in this study are four solvents (EC, PC, EMC, and DMC) and two salts ($LiPF_6$ and LiTFSI) among those most frequently used in batteries. We also selected two ionic liquids comprising the same $TFSI^-$ anion associated to the two homologous cations: the ammonium (methyl butyl-pyrrolidinium) and the phosphonium (methyl tributyl-phosphonium) group. **Table 1** and **Table 2** give the name, structure, and charge distribution of the solvents and salts selected for this study, respectively. The electrolyte formulations with a binary mixture of EC/EMC or EC/DMC, and a ternary mixture of EC/PC/DMC or EC/PC/EMC enabled comparison of the measurements by revealing the role of each solvent. The concentration of the tested salts was kept at 1mol/L and the ionic liquids were added to (EC/EMC + 1mol/L) in mass proportions of 5% and 30%.

**Table 1**. Name, structure, and charge distribution of the alkylcarbonate used in this study

| | EC | PC |
|---|---|---|
| Cyclic alkylcarbonates | 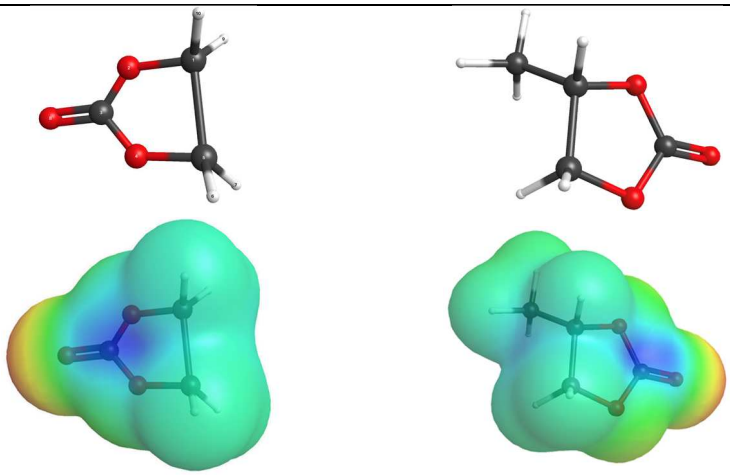 | |
| | EMC | DMC |
| Linear alkylcarbonates | 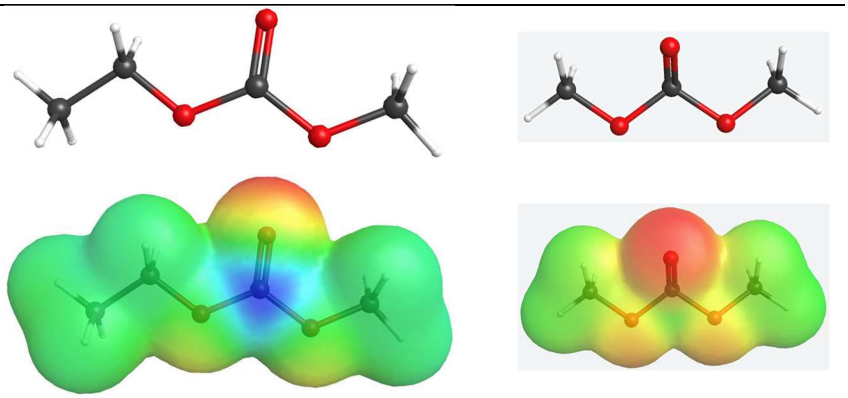 | |

**Table 2**. Name, structure, and charge distribution of the ions for salts and ILs used in this study

| Salt's anions | $PF_6^-$ | $TFSI^-$ |
|---|---|---|
| Name | Hexafluoro phosphate | bis (trifluoro-sulfonyl) imide |
| Structure | 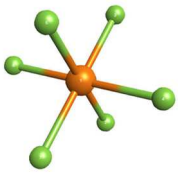 | 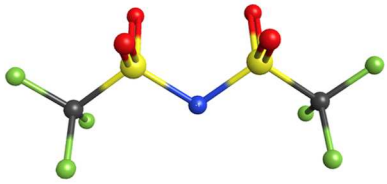 |
| Charge distribution | 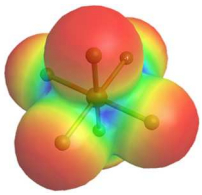 | 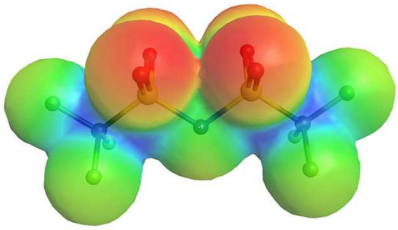 |
| **Liquid ionic's cations** | $Pyrr_{14}^+$ | $Phos_{1444}^+$ |
| Name | Methyl butyl-pyrrolidinium | Methyl tributyl-phosphonium |
| Structure | 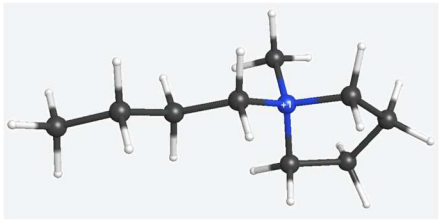 | 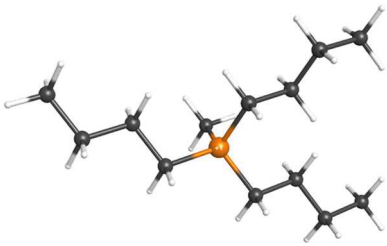 |
| Charge distribution | 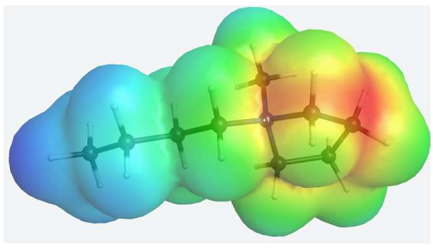 | 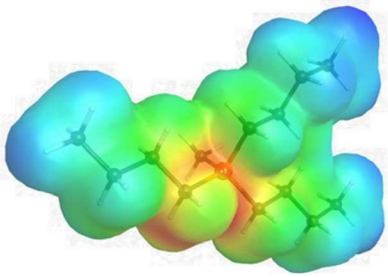 |

The gases that form in batteries have several origins, such as the materials themselves, and the electrolytes. The use of graphite requires the formation of an SEI (Solid Electrolyte Interphase) which causes the formation of several gases, resulting from low potential chemical and electrochemical decomposition reactions of alkylcarbonates, catalyzed by

graphite. These reactions lead to the formation of several gases including ethene ($C_2H_4$), carbon dioxide ($CO_2$), or dioxygen ($O_2$), according to the following mechanisms:

$$2C_3H_4O_3 + 2\,Li^+ + 2e^- \longrightarrow \mathbf{C_2H_4} + [CH_2OCO_2Li]_2 \quad \text{(eq1)}$$

$$2C_3H_4O_3 + 2\,Li^+ + 2e^- \longrightarrow \mathbf{CO_2} + [C_2H_4OLi]_2 \quad \text{(eq2)}$$

$$[CH_2OCO_2Li]_2 \longrightarrow \mathbf{CO_2} + \mathbf{C_2H_4} + Li_2CO_3 + \frac{1}{2}\mathbf{O_2} \quad \text{(eq3)}$$

The NMC cathode is a metal oxide. These materials are known to release dioxygen by high potential oxidation. The dioxygen produced can then react with the solvents to give $CO_2$:

$$2{,}5\,\mathbf{O_2} + C_3H_4O_3 \longrightarrow 3\,\mathbf{CO_2} + 2\,H_2O \quad \text{(eq4)}$$

To compare the effects of the solvent salts and the ionic liquids, the same program was applied to the Gr//NMC pouch cells, and is summarized in **Table 3**. Whatever the electrolyte composition, the first cycle for SEI formation was carried out at 60 °C, at C/20, corresponding to a mass current density of J = 8.5 $mA.g^{-1}_{NMC}$. These conditions were chosen in order to favor the formation of a good SEI which ensures efficient cycling thereafter.

**Table 3**. Gr//NMC pouch cycling program

| Cycle | C-rate | Temperature | ΔE range (V) |
|---|---|---|---|
| **1** | C/20 | 60 °C | |
| **2-6** | C/5 | 25 °C | |
| **7-16** | C/1 | 25 °C | 2.9 – 4.2 |
| **17-22** | C/2 | 40 °C | |
| **23-27** | C/5 | 25 °C | |

*4.1. Comparative effect of DMC and EMC on gas generation*

**Figures 4a and 4b** compare the galvanostatic profiles of pouch cells comprising the two binary mixtures (EC / DMC: 1 /1 + 1M $LiPF_6$) and (EC / EMC: 3/7 + 1M $LiPF_6$) at different regimes. For each electrolyte two parallel measurements were made and are represented by the different cell numbers, for example Cell 202 and 203 in the case of EC/DMC as shown in (**Figure 4c**).The electrochemical performances obtained for the two electrolytes based on a binary mixture of alkyl carbonates are very close.

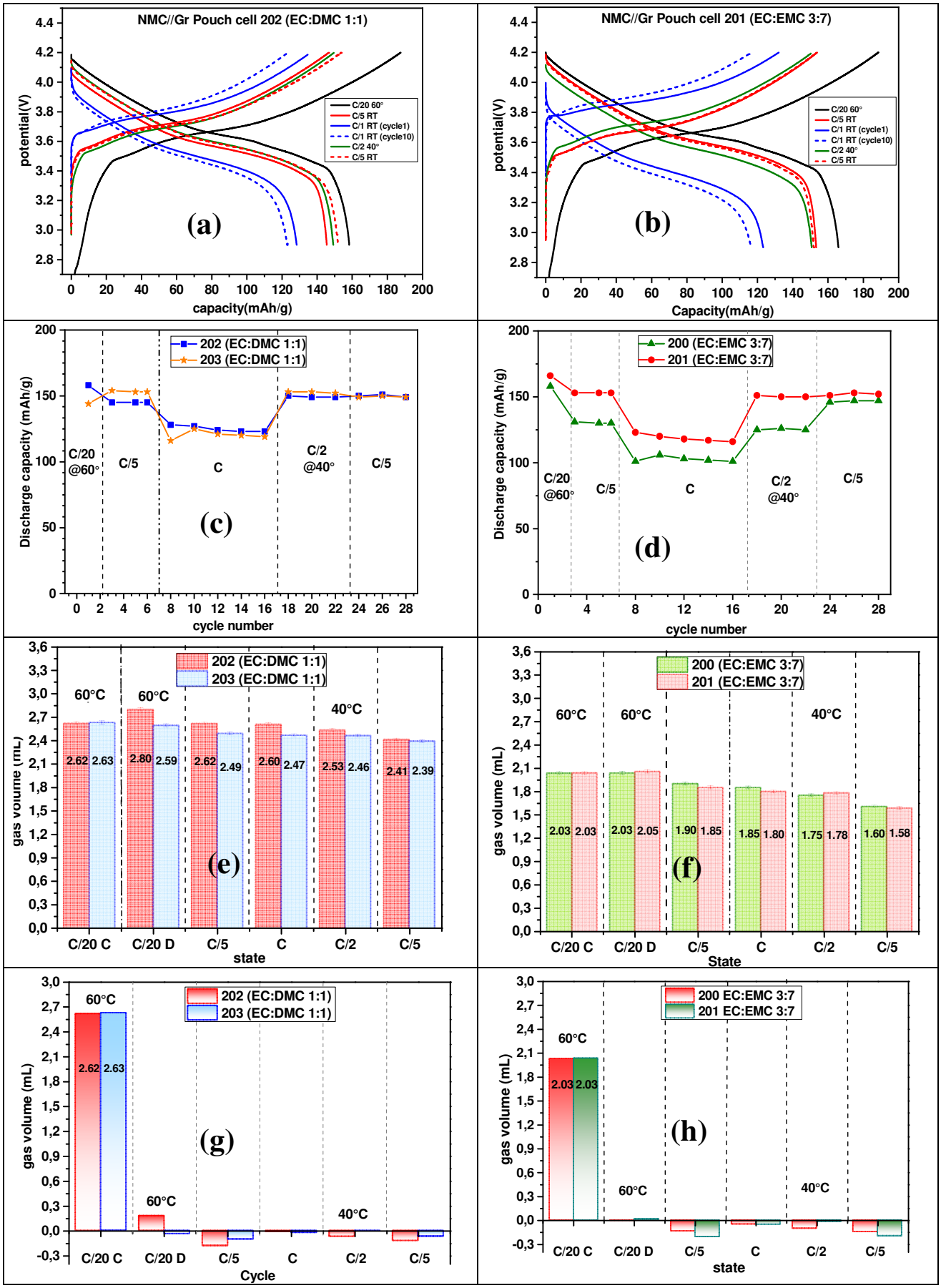


**Figure 4**. Comparative electrochemical and gas volume characterizations for Gr//NMC with (EC/DMC: 1/1 + 1M $LiPF_6$) and (EC/EMC: 3/7 + 1M $LiPF_6$).

The first cycle at C/20 shows an irreversible capacity of approximately 22 $mAh.g^{-1}$ which represents 13% to 14% of the total initial charge capacity, 170 $mAh.g^{-1}$ for (EC / EMC: 3 /7 + 1M $LiPF_6$) and 160 $mAh.g^{-1}$ for (EC / DMC: 1/1 + 1M $LiPF_6$), respectively. These values are consistent with the irreversible and initial capacities reported in the literature, i.e. between 10% and 20% [27, 28]. For both electrolytes, the retention capacity evaluated when returning to a C/5 regime (cycle 23) was high (> 99%). At high current density, (C/1), the capacity remained stable around 120 $mAh.g^{-1}$. During the formation of the SEI on graphite in the first cycle, the average volume of gas released in the case of the cell based on (EC / DMC: 1/1 + 1M $LiPF_6$) was 2.62 ± 0.03 mL ( **Figure 4 e**), 31% higher than in the case of (EC / EMC: 3/7 + 1M $LiPF_6$) (**Figure 4 f**). The gas is mainly formed during the first charge. The cumulative volume dropped slightly during the cycles. This phenomenon is more visible on the representation of the volume generated per cycle (**Figure 4 g, 4 h**), and can be attributed to the slow dissolution of the gas released in the electrolyte as well as to the reactivity of less soluble gases such as $O_2$ in favor of $CO_2$, which is more soluble (eq. 4). No significant change was observed at 40 ° C for the two electrolytes. After 27 cycles, the pouch cell containing (EC / DMC: 1/1 + 1M $LiPF_6$) was 51% more swollen than that which cycled with (EC / EMC: 3/7 + 1M $LiPF_6$). There is a definite advantage in working with EMC instead of DMC for obvious safety reasons.

*4.2. Effect of PC in alkylcarbonate ternary mixture on gas generation*

The comparison of the performances during the first 27 cycles and their correlation with the gases generated, expressed in cumulative volume (v in mL), is collated in **figure 5** (a-f). As in the case of binary mixtures, the performances of the two ternaries were similar, with initial capacities of 155 $mAh.g^{-1}$ and 165 $mAh.g^{-1}$ in the presence of DMC and EMC, respectively. After 27 cycles, at different regime, 98% of the initial capacity is recovered. The difference with the performances observed with the binary mixture is the behavior with strong current density. This result is logical given that PC is viscous ($\eta$ = 2.93 cP at 20°C) [29] and disfavors the rapid diffusion of $Li^+$ ions. Concerning gas formation, the addition of PC does not drastically modify the observations noted in the case of binary mixtures: (i) the DMC generates more gas (+ 25%) than EMC, (ii) and the cycles carried out at 40 °C do not increase the formation of gas. In addition, the absolute quantity of gas measured with and without PC is very close. This result means that PC does not participate in the decomposition reactions of alkylcarbonates which form gases (eq. 1-4). In summary, among the 4 solvents tested here, it is essentially EC which is at the origin of the quantities of gas measured. We

can therefore establish the following classification of the 4 solvents with respect to their respective gas-forming roles: EC> DMC> EMC> PC. This result was expected as EC is responsible for the formation of the SEI and it is at this stage of battery life that the majority of gases are formed.

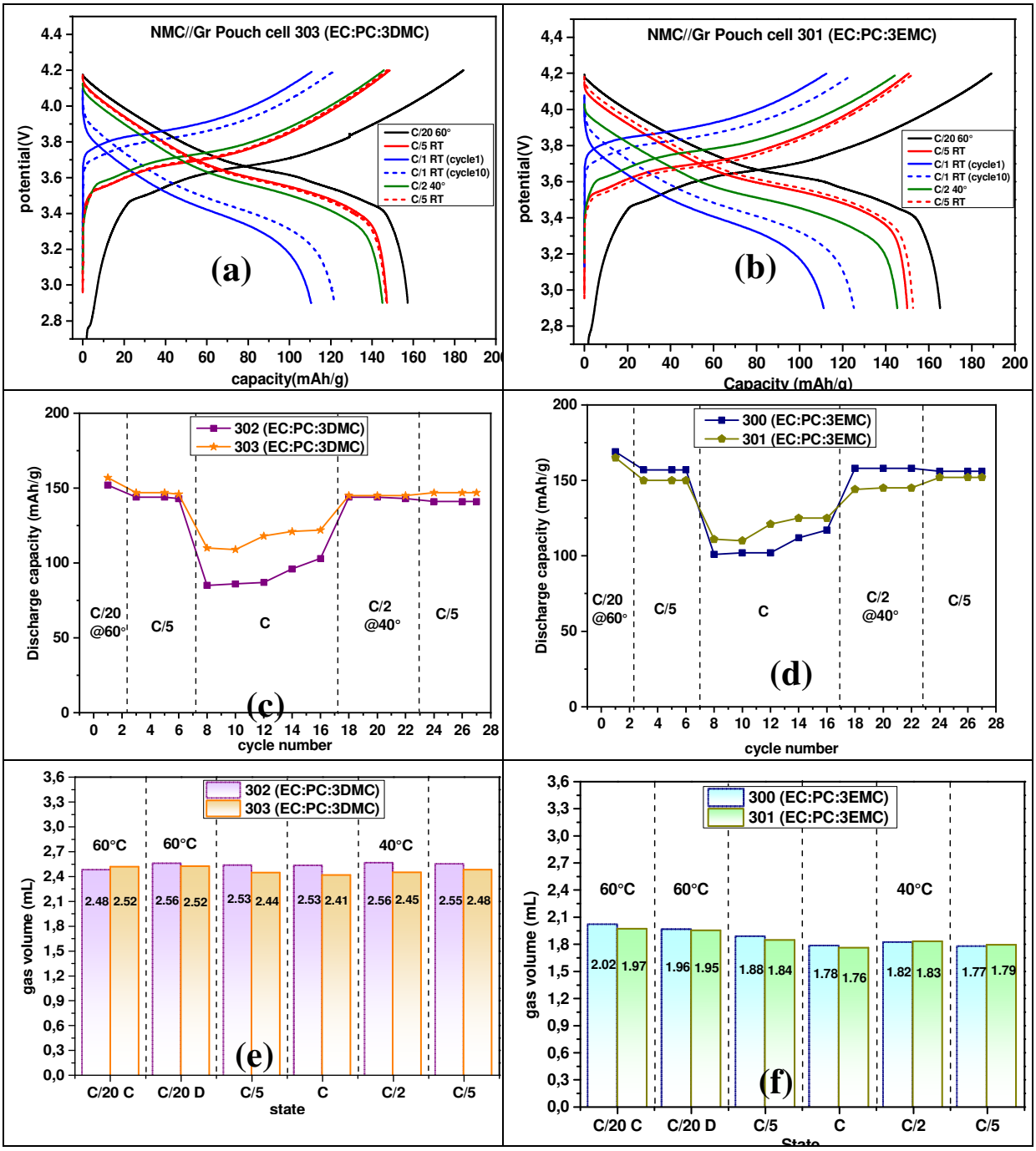


**Figure 5.** Comparative electrochemical and gas volume characterizations for Gr//NMC with (EC/PC/3DMC + 1M $LiPF_6$) and (EC/PC/3EMC + 1M $LiPF_6$).

The SEI formation and the gas generated in significant quantities generally leave traces on the layer. After cycling, the surface of the materials undergoes a transformation which carries

the stigmata of deposits, cracks due to mechanical stresses or gas diffusion, and agglomeration zones of particles following a migration of transition metals.

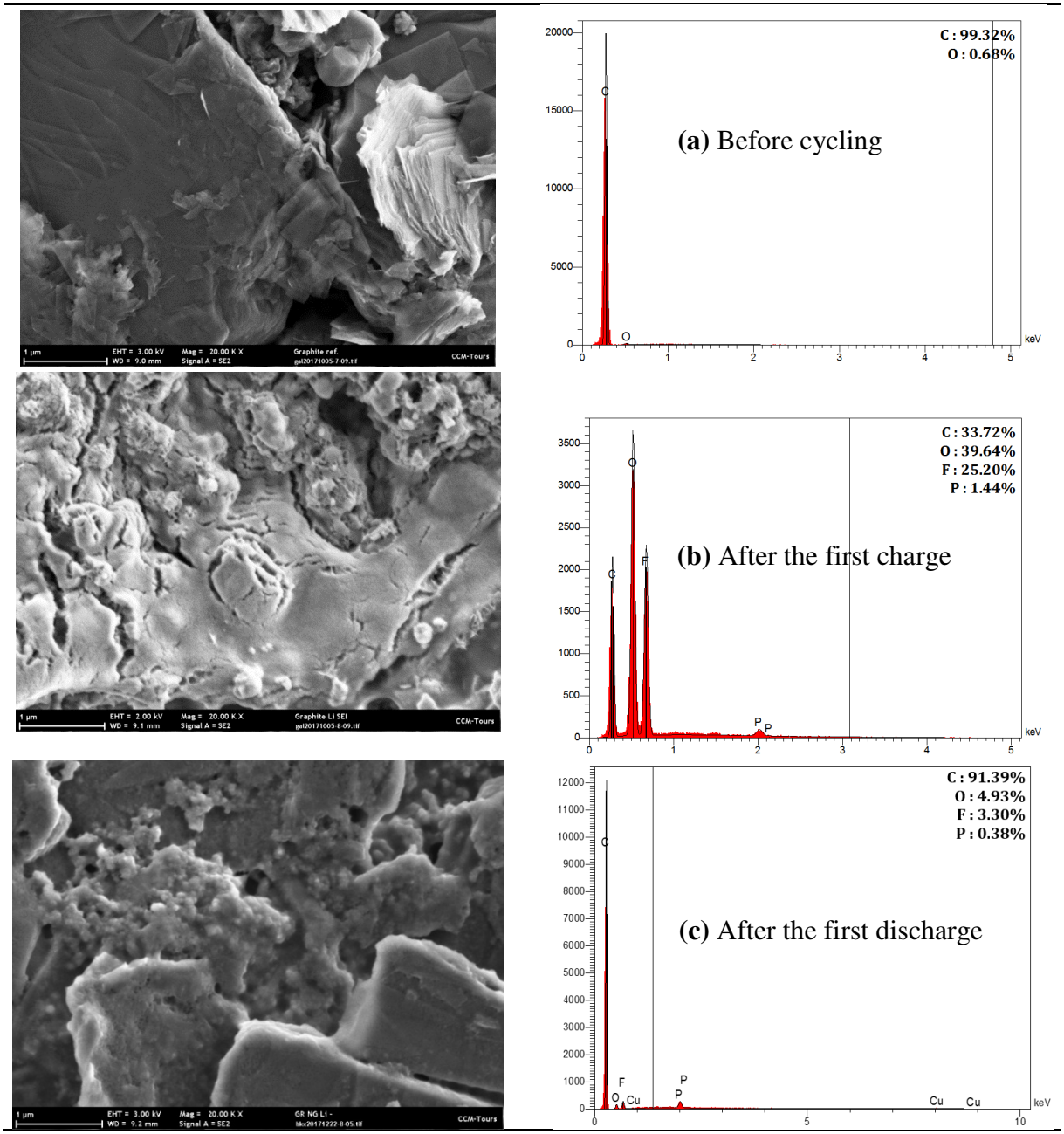


**Figure 6.** SEM images at the same magnification (x 20.000) and associated EDX of a graphite electrode cut of a pouch cell of the Gr//NMC system at different stages of the first cycle in the presence of (EC/PC/3DMC + 1M $LiPF_6$).

Scanning electron microscopy associated with an energy dispersion spectrometry microanalysis (EDX) was carried out. The latter is based on the detection of X photons, offering the possibility of observing the SEI. **Figure 6** presents the SEM and EDX

radiographs of the graphite surfaces cut on pouch cells (a) before cycling (b) at the end of the first charge and (c) at the end of the first discharge.

The graphite used in this study is artificial. Before being cycled (**Figure 6 a**), it presents a striated appearance where the "scales" characteristic of graphite morphology can be seen [30]. These consist of stacks of graphene sheets which measure approximately 10 µm. There is no particular organization of these clusters. On the other hand, the graphene sheets are clearly observed. Quantification by EDX reveals a carbon content of 99.32% with a low proportion of oxygen, less than 1%. On lithiated graphite (**Figure 6 b**), it is no longer possible to see graphene sheets because they are covered by a homogeneous layer of SEI obtained by the reduction of solvents and salts during the first lithiation. Quantification by EDX analysis evaluated the level of visible carbon at the surface to be only 33.72%, oxygen 39.64%, fluorine 25.20% and phosphorus 1.44%. These elements account for the composition of the SEI, in particular by mineral compounds of the LiF, $Li_2CO_3$ type or the organic part (lithium alkoxides and polycarbonates) [31]. On the other hand, on the lithiated graphite, discontinuities of the SEI in the form of cracks are visible. These cracks in the passivation layer are created by the evacuation of gases generated by the formation of the SEI [32].

On the graphite discharged during the first cycle (**Figure 6 c**), characteristic graphite grains can be seen because the SEI is partially dissolved. This was confirmed by the quantification by EDX which revealed a significant proportion of carbon (91.39%) but which remains lower than that measured on the virgin graphite electrode (> 99%), which means that there remains a thin film of SEI on the surface of the graphite. It is then clear from these SEM pictures and their corresponding EDX analysis that the passivation layer evolves throughout the battery lifetime as shown by XPS [33] during the charge-discharge cycles and that at least part of the formation / dissolution of the SEI continues throughout the cycling.

### *4.3. Comparative effect of $LiPF_6$ and LITFSI salts on gas generation with temperature*

**Figure 7** compares the gases measured during the cycling of two ternary mixtures of EC/PC/ 3DMC solvents comprising either 1M $LiPF_6$ or 1M LiTFSI at two temperatures, 25 °C and 40 °C. The first SEI training cycle was always carried out at 60 ° C. During this first cycle, LiTFSI formed 35% more gas than $LiPF_6$, probably because its passivation layer is thicker. For the rest of the cycles, while at 25 °C, the quantity of gas changed little, at 40 °C, in the presence of LiTFSI the volume of gas generated decreased in particular during the rapid

cycles at C /1. A rational explanation for these observations is the slow dissolution of the gas generated during the first charge. This dissolution will depend on two parameters: the nature of the salt and the temperature. The solubility of gases such as $O_2$, $H_2$, $CO_2$, $CH_4$ and $C_2H_4$ in battery electrolytes is an endothermic phenomenon which is favored by temperature [22]. It is therefore logical to observe a decrease in the volume of gas with temperature. On the other hand, the nature of the lithium salt has a distinct effect on the solubility of gases in carbonate-based electrolytes.

We have shown in previous work [18-21] that salt plays a decisive role in the dissolution mechanism of $CO_2$ in electrolytes. $LiPF_6$ has a rather negative effect on the $CO_2$ dissolution process, so-called salting-out, while LiTFSi has a rather positive effect, called "salting-in". For example, at 80 °C in the DEC, the Henry constant, which is inversely proportional to the molar fraction of gas dissolved in the electrolyte, $K_H$ = 12.66 MPa without salt, becomes $K_H$ = 18.14 MPa in the presence of $LiPF_6$ and remains unchanged $K_H$ = 12.28 MPa in the presence of LiTFSi [18]. The effect of gas solubility in electrolytes will be discussed further in section *4.5.2*.

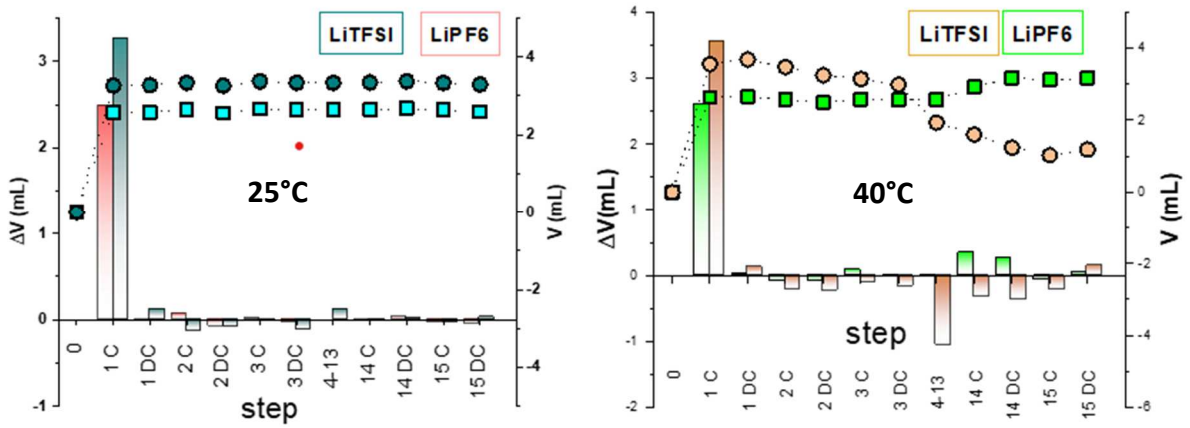


**Figure 7.** Comparison of variations in the volume of Gr//NMC pouch cells with EC/ PC/3DMC + 1 mol.$L^{-1}$ LiX (X = $PF_6$ or TFSI) as a function of temperature.

The explanation of this opposite effect on the solubility of gases according to the nature of the salt is the delocalized and elongated structure of the $TFSI^-$ anion which allows empty cavities in the structure of the mixture (solvents + salt) and thus allows the introduction of a quadrupole such as the $CO_2$ molecule. This means that after the gases have been generated during the initial stage of preparation of the SEI, they are slowly dissolved in the electrolyte, all the more so since the salt has a salting-in power as here LiTFSI. In conclusion, the effect of salt on the swelling of cells can be summarized as follows: (i) the consumption by

dissolution of the gases generated could be a positive point for the safety of the batteries by reducing the pressure; (ii) the solubility of the gases is very different according to their nature and it is the most soluble gases that are favored by the presence of TFSI-; (iii) despite the interest of TFSI in the solubility of gases, $LiPF_6$ provides a higher SEI quality and consequently a higher performance.

### *4.4. Effect of ionic liquids on gas generation*

Ionic liquids can be considered as the other salts of the electrolyte ($LiPF_6$ and LiTFSI) except that their cation, which differs from $Li^+$, does not participate in capacity. Their role is predominant at the polarized interface due to their ionic character. They also improve the transport properties of the electrolyte and its thermal characteristics depending on the quantities added. The solubility of gases can also be influenced by ionic liquids as shown by many studies [34-37]. We chose here an ammonium and a phosphonium at two concentrations, 5% and 30%, to distinguish their effect as additives (5%) and co-solvent (30%).

#### *4.4.1. Effect of $Phos_{1444}$ TFSI on gas formation*

It was found that phosphonium ILs exhibited lower viscosities, higher conductivities and thermal stabilities than those of the corresponding ammonium [38-40]. However, most of the work reporting the introduction of these ionic liquids concerns half-batteries with a lithium anode [38, 39]. Graphite, with the formation of SEI, a key and delicate stage, is more sensitive to the introduction of additives comprising groups capable of reducing at low potential such as phosphonium. **Figure 8** shows the electrochemical performances as well as the gas volumes measured with a binary mixture (EC / EMC: 3/7 + 1M $LiPF_6$) comprising (0%, 5% and 30%, by mass) of $Phos_{1444}$ TFSI (named IL1). A significant increase in irreversible capacity is observed with the addition of ionic liquids (**Figure 8 a, b**) which goes from 13% (section 4.1) to 20% then 37% for 0%, 5% and 30 % of $Phos_{1444}$ TFSI, respectively. The consumption of the electrolyte during the stage of SEI formation results in the generation of larger quantities of gas. For 5%, the quantity of gas measured increases by 30% compared to the reference without IL (**Figure 8 c, f**), i.e. 2.65 mL and 2.02 mL. With 30% ionic liquid (**Figure 8 d**), the quantity of gas formed is almost multiplied by 3, with 5.78 mL (**Figure 8 d**).

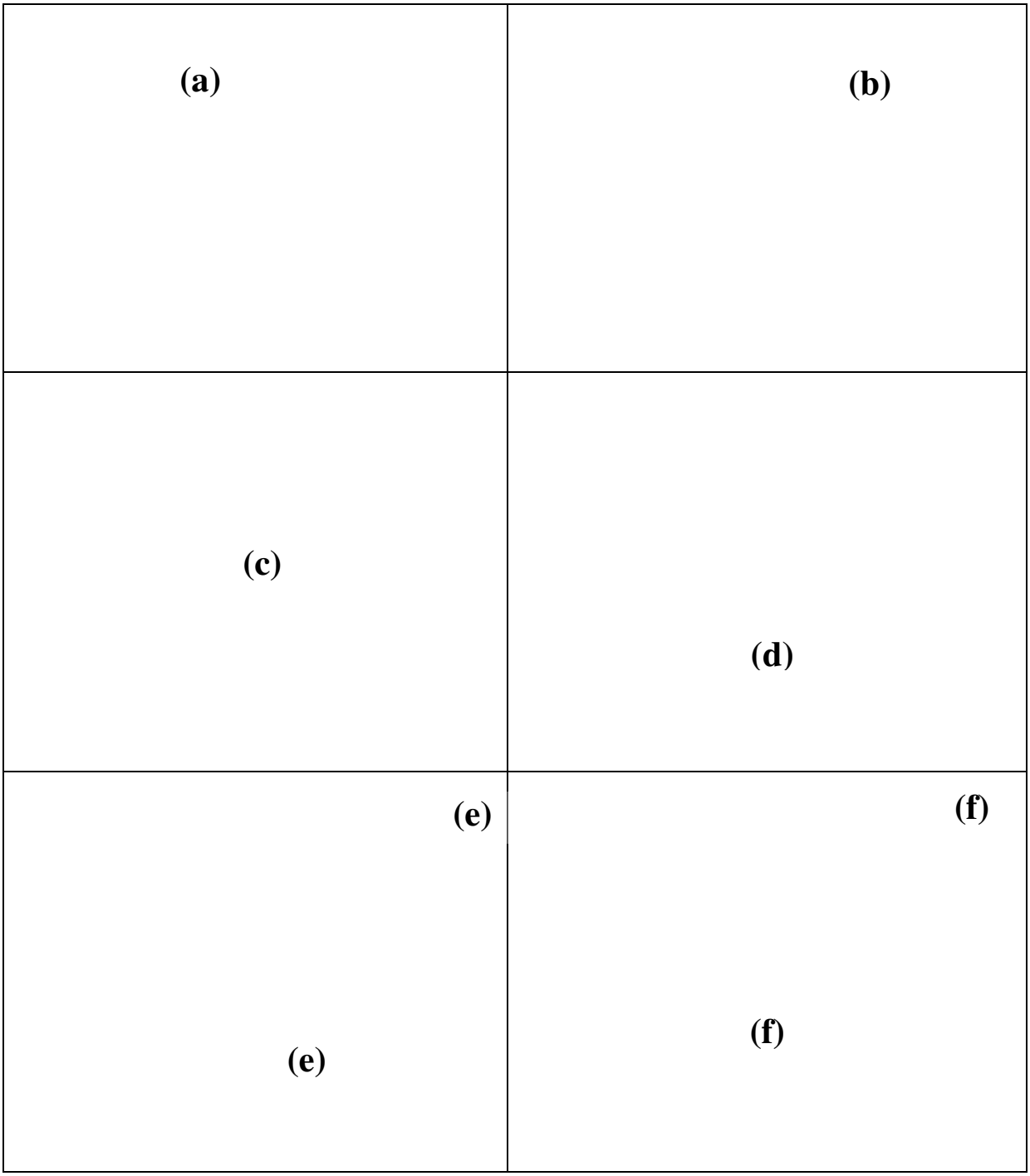


**Figure 8.** Comparative electrochemical and gas volume characterizations for Gr//NMC with (3EC/ 7EMC + 1M $LiPF_6$) with 5 % and 30 % in mass of $Phos_{1444}TFSI$ (denoted IL1).

The performance of pouch cells at different current densities is also correlated with the high generation of gas when ionic liquid is added (**Figure 8 e**). In fact, adding 30% of ionic liquid reduces the capacity by 50% at low C-rate (C / 1). This result is expected due to the size of the alkyl phosphonium cation and its diffusion in the electrolyte. In addition, its polarity promotes its adsorption on the surface of the graphite under load and catalyzes the reduction reactions.

### 4.4.2. *Effect of Pyrr$_{14}$ TFSI on gas formation*

**Figure 9** shows the performance of Pyrr$_{14}$ TFSI (denoted IL2) in the same compositions as Phos$_{1444}$ TFSI (5% and 30%, by mass) and compares its performance with that of the reference, without ionic liquid. First of all, the electrochemical performances for the three compositions (0, 5 and 30%) are close to or slightly higher in favor of 5% Pyrr$_{14}$ TFSI (**Figure 9 e**) with initial capacities of 160 and 140 mAh.g$^{-1}$ at C/20 for 5 and 30% respectively (**Figure 9 a, b**), although the reversible capacity is greater (28 mAh.g$^{-1}$ for 5%, and 47 mAh.g$^{-1}$ for 30%).

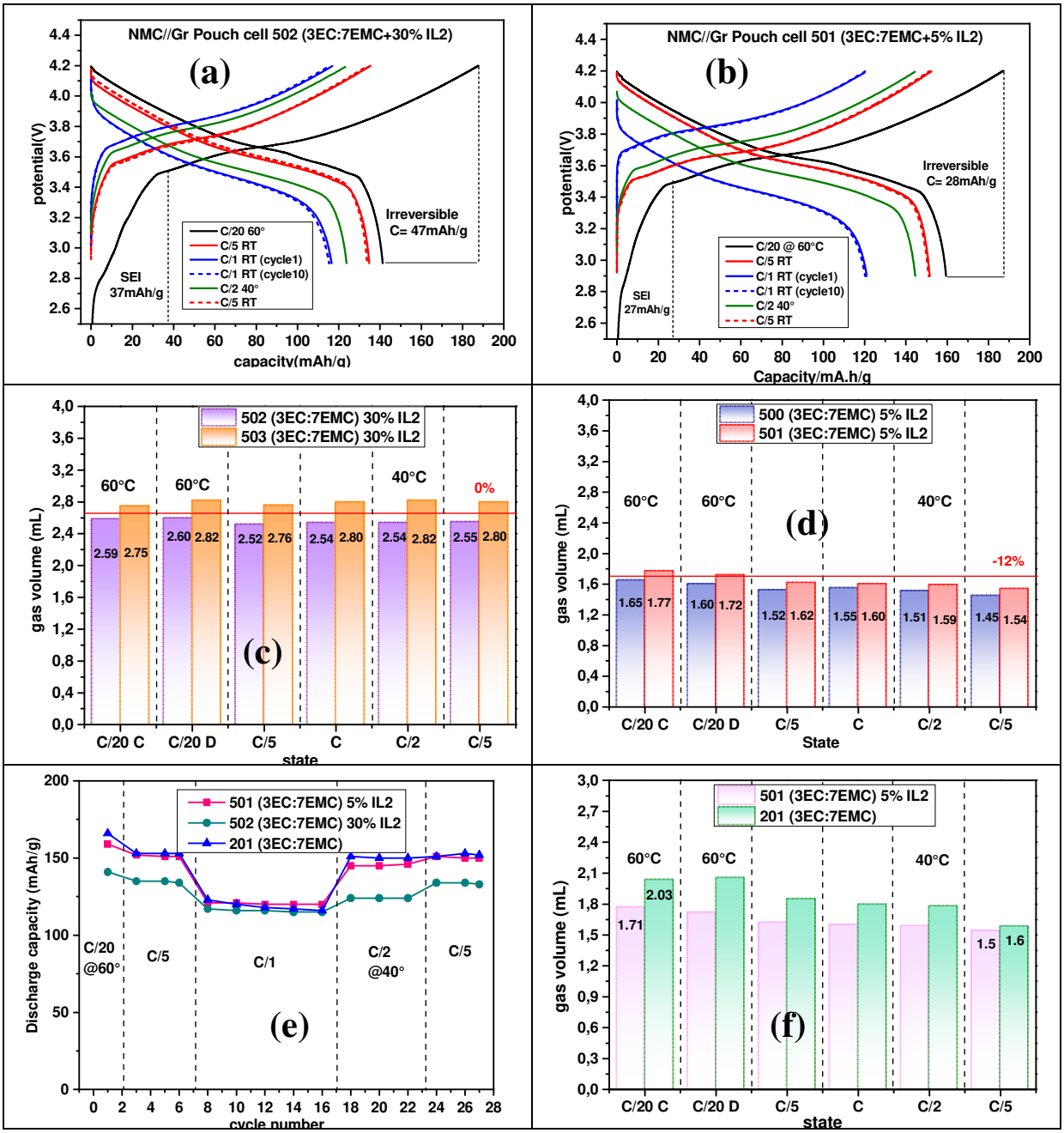

**Figure 9.** Comparative electrochemical and gas volume characterizations for Gr//NMC pouch cells with 1 mol.L$^{-1}$ $LiPF_6$ in 3EC /7EMC with 5 % and 30 % in mass of $Pyrr_{14}TFSI$ (denoted IL2).

The addition of $Pyrr_{14}$ TFSI 5% seems to limit the formation of gas (**Figure 9 d, f**) by 16% by reducing the volumes measured under the same conditions. For the largest quantity of ionic liquids, 30%, the gases formed at the first charge are 25% greater than those of the reference without ionic liquid, and this quantity of gas does not vary throughout the cycling (**Figure 9 c**). The addition of ionic liquids to the electrolytes is appreciated in the field of batteries because it helps to decrease the flammability of the electrolytes and increases the working temperature window, provided that it does not prevent cycling. From this point of view, $Pyrr_{1444}$ TFSI plays its role perfectly for the two proportions tested, and $Phos_{1444}$ TFSI to a lesser extent when 5% by mass is added in the electrolyte.

### *4.5. Analysis of Gases on pouch cell and their solubility in the electrolyte*

#### *4.5.1. Nature of the gases as a function of temperature*

In order to complete these quantitative results of the volumes of gas generated, an analysis of the composition of the gases collected in the pouch cells was carried out by gas chromatography coupled with mass spectroscopy (GC-MS). This analysis was performed several weeks after the cycling of the pouch cells had stopped, so we consider that the solubility equilibrium of the gases had been reached. The results for the two systems (EC/PC/3DMC + 1M $LiPF_6$) and (EC/PC/3DMC + 1M LiTFSI) at three temperatures are collated in **Figure 10**.

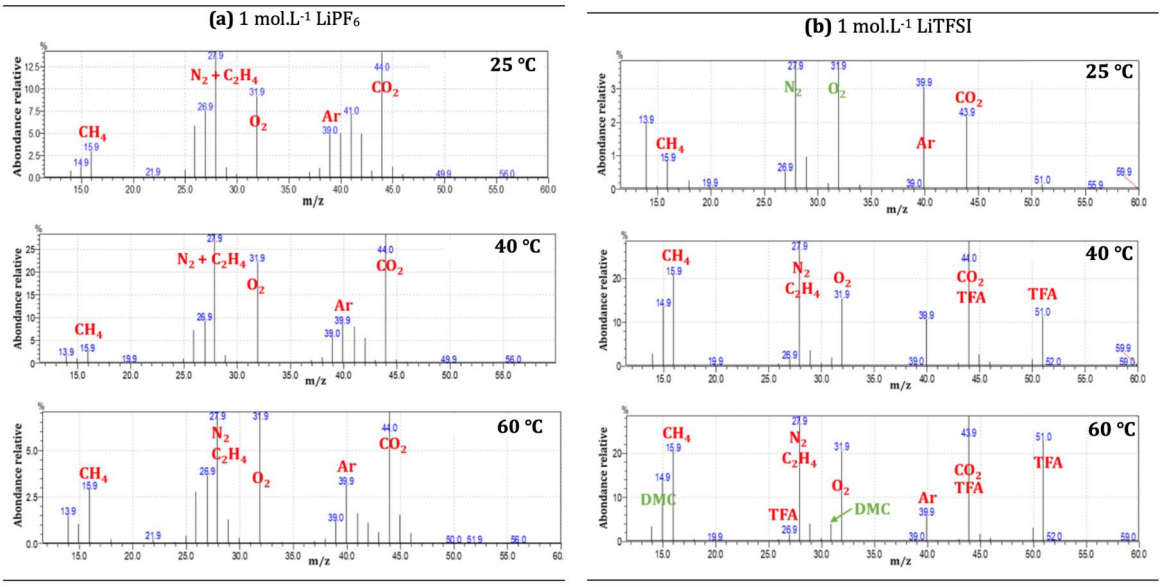

**Figure 10** GC-MS analysis of Gr//NMC pouch cells with (EC/PC/3DMC + 1M $LiPF_6$) and (EC/PC/3DMC + 1M LiTFSI) cycled at different temperatures.

Composition analysis of the gas taken from a Gr//NMC pouch cell, cycled at 25 ° C. with (EC/PC/3DMC + 1M $LiPF_6$), shows (**Figure 10 a**) that the most intense peak is at m / z = 44, which corresponds to carbon dioxide $CO_2$. The ratio of the peaks at 27.9 and 31.9 is higher than the $N_2/O_2$ proportion in the calibration (air). The $CH_4$ peak is also visible with a relative abundance of around 3% here. By comparison, the results obtained with LiTFSI show very little $CO_2$ and $CH_4$ even though the overall quantity of gas measured at the end of the cycling was equivalent for the two salts (2.4 to 2.9 ml). This confirms the hypothesis that we proposed previously, namely that a large part of the gas generated in the presence of LiTFSI salt is dissolved in the electrolyte and is therefore not detectable by GC-MS.

At 40 °C, the peaks found with $LiPF_6$ are identical to those observed at 25 °C with higher intensities, in particular the peaks at m / z = 27.9 relative to $C_2H_4$ and / or (CO). The relative abundance of $CO_2$ here is 65% compared to $C_2H_4$/CO. In the presence of LiTFSI, characteristic peaks at m / z = 16, 44, 51 and 69 are observed; they correspond to the presence of trifluoroacetamide originating from the degradation of the $TFSI^-$ anion. At 60 °C, the relative abundances increase. In the case of $LiPF_6$, the most intense peak remains that of $CO_2$, while for LiTFSI, the intensities of the $CO_2$ peaks are lower than at 25 ° C or 40 ° C. This confirms the previous hypothesis that the solubility of gases in the presence of LiTFSI is favored by temperature.

### *4.5.2. Gas solubility in electrolyte as a function of temperature*

**Figure 11** depicts the measured solubilities of oxygen and of dihydrogen expressed in the Henry constant, obtained in pure propylene carbonate (**figure 11 a**) and dimethyl carbonate (**figure 11 b**) as a function of temperature. From the four solvents used, we chose a cyclic alkylcarbonate (PC) and a second linear alkylcarbonate (DMC) for comparison. The results obtained in DMC were compared with those obtained by Kolar et al. [41], while the measurements obtained for $CO_2$ and $CH_4$ were carried out in our previous work [18].

The very low solubilities of $O_2$ and $H_2$ compared to that of $CO_2$ are similar in the two solvents. The results obtained in propylene carbonate show that the solubility of $H_2$ and $O_2$ decreases with temperature, as do $CO_2$ and $CH_4$. The solubility in both solvents increases in the following order: $O_2 < H_2 < CH_4 < CO_2$. In DMC, unlike $CO_2$ and $CH_4$, whose solubility

decreases in this solvent, $H_2$ and $O_2$ show an opposite tendency. For $CO_2$ and $CH_4$, solubility is an exothermic process which decreases with temperature [33-35], whereas in the case of $O_2$ and $H_2$, dissolution in the alkylcarbonate corresponds to an endothermic process.

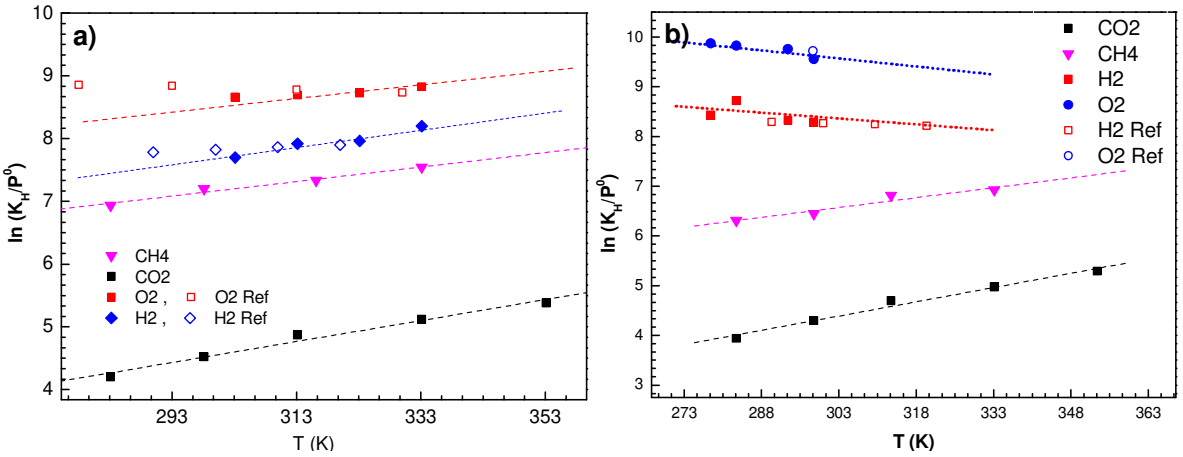


**Figure 11**. Solubilities of $O_2$ and $H_2$ measured in PC (a) and DMC (b), obtained in this work and compared with [41] (named ref) and comparison with the solubilities of other gases [18, 20, 21].

These observations on the solubility of gases lead to two important conclusions for our study: (i) the two gases responsible for the swelling of the salts are those which are the least soluble, and not necessarily the most abundant, i.e. $O_2$ and $H_2$; ( ii) the temperature affects the solubility of gases differently depending on the nature of the alkylcarbonate (PC or DMC). The solubility of gases follows the order: $CO_2$> $CH_4$> $C_2H_4$ >> $O_2$ ~ $H_2$.

We also measured the solubility of ($O_2$ and $H_2$) in the ternary mixture EC/PC/3DMC with and without salts ($LiPF_6$ and LiTFSI). **Figure 12** shows the compared solubility expressed with the Henry constant $k_H$ of $H_2$ (**Figure 12 a)** and $O_2$ **(Figure 12 b)** in the three systems.

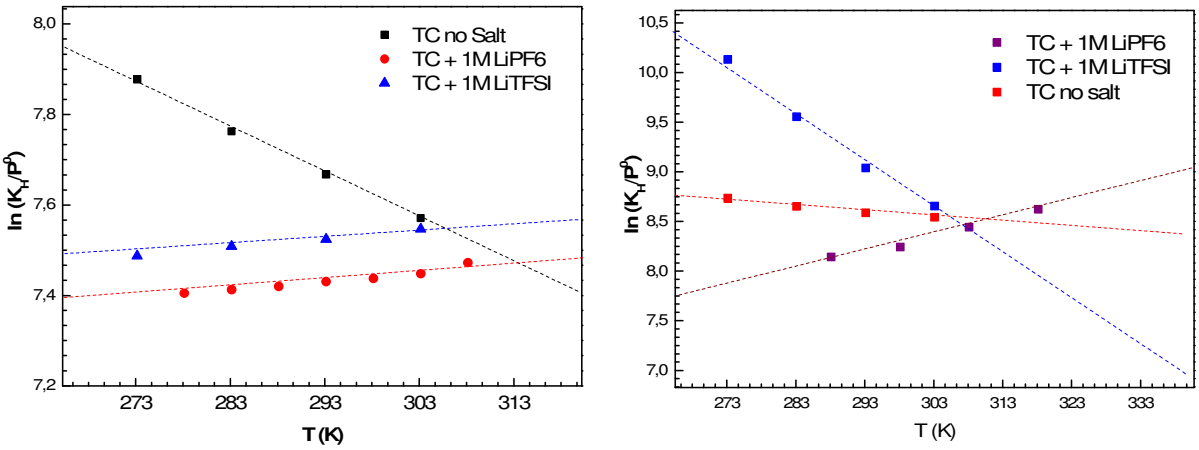

**Figure 12**. Effect of the lithium salt on the solubility of $H_2$ (a) and $O_2$ (b) in the ternary mixture EC / PC/3DMC 1 M LiX (X = $PF_6$ or TFSI).

It should be noted that for the two gases, in the ternary mixture without salts, there is a decrease in solubility with temperature. In the case of $H_2$, the two salts have a "salting in" effect and correspond to endothermic processes favored by temperature. With $O_2$, at low temperature, the solubility is greater with LiPF6 than with LiTFSI, but this tendency is reversed with the temperature from 40 °C. These solubility measurements tell us about the ability of the electrolytes to dissolve part of the gases formed during cycling to avoid excessive swelling of the cell pouches. We can summarize this trend by concluding that LiTFSI is interesting at high temperatures and for systems that generate large amounts of gases such as cathodes based on transition metal oxides.

## Conclusion

In this study, we evaluated the gas volumes in the Gr//NMC system for various electrolyte compositions as a function of temperature. An original device allowing the volumes of gas to be quantified at each cycle, and the analysis of their nature at the end of cycling allowed us to compare the systems studied with good repeatability and reliability. We evaluated the effects of salts, solvents and ionic liquids on the amount of gas formed. The results made it possible to determine the quantity of gas produced and to show that it is essentially linked to the formation of the SEI at the first charge. It is greater in the case of LiTFSI compared to $LiPF_6$ (2.8 mL vs 1.9 mL). These observations on the quantities of gas were correlated with the solubility of gases in the electrolyte. LiTFSI allows a "salting in" effect which physically results in the wilting of the pouch cells and a reduction in the volume of gas during cycling. This phenomenon, attributed to a better solubility of the gases produced in the electrolyte in the presence of this salt, is accentuated with temperature. Analysis of the gas composition by GC-MS revealed a predominance of $CO_2$ and $CH_4$ gases and confirmed the effect of salt in the quantity and composition of the gas mixture. In conclusion, ILs and LiTFSI are interesting at high temperatures and for systems that generate large amounts of gases such as cathodes based on transition metal oxides.

## Acknowledgements

The authors would like to thank "La Région Centre Val de Loire" and "Le Studium Loire Valley Institute for Advanced Studies" for financial support through the Obama project under the Lavoisier regional program. We would also like to thank Dr. Pierre-Yvon Raynal at the

Faculty of Medicine in Tours for SEM analyses and Frédéric Montigny from the Scientific and Technical Platform of the University of Tours for GC/MS characterization of the samples.

## References

[1] F. Diaz, Y. Wang, R. Weyhe, B. Friedrich, Gas generation measurement and evaluation during mechanical processing and thermal treatment of spent Li-ion batteries, Waste Management, 84 (2019) 102-111.
[2] J.H. Seo, J. Park, G. Plett, A.M. Sastry, Gas-Evolution Induced Volume Fraction Changes and Their Effect on the Performance Degradation of Li-Ion Batteries, Electrochemical and Solid-State Letters, 13 (2010) A135.
[3] L. Wang, W. Choi, K. Yoo, K. Nam, T.J. Ko, J. Choi, Stretchable Carbon Nanotube Dilatometer for In Situ Swelling Detection of Lithium-Ion Batteries, ACS Applied Energy Materials, 3 (2020) 3637-3644.
[4] E. Fan, L. Li, Z. Wang, J. Lin, Y. Huang, Y. Yao, R. Chen, F. Wu, Sustainable Recycling Technology for Li-Ion Batteries and Beyond: Challenges and Future Prospects, Chemical Reviews, (2020).
[5] C.P. Aiken, J. Self, R. Petibon, X. Xia, J.M. Paulsen, J.R. Dahn, A Survey of In Situ Gas Evolution during High Voltage Formation in Li-Ion Pouch Cells, J. Electrochem. Soc., 162 (2015) A760-A767.
[6] M. Woody, M. Arbabzadeh, G.M. Lewis, G.A. Keoleian, A. Stefanopoulou, Strategies to limit degradation and maximize Li-ion battery service lifetime - Critical review and guidance for stakeholders, Journal of Energy Storage, 28 (2020) 101231.
[7] L.H.J. Raijmakers, D.L. Danilov, R.A. Eichel, P.H.L. Notten, A review on various temperature-indication methods for Li-ion batteries, Applied Energy, 240 (2019) 918-945.
[8] L. Zhang, P. Zhao, M. Xu, X. Wang, Computational identification of the safety regime of Li-ion battery thermal runaway, Applied Energy, 261 (2020) 114440.
[9] S. Xie, L. Ren, X. Yang, H. Wang, Q. Sun, X. Chen, Y. He, Influence of cycling aging and ambient pressure on the thermal safety features of lithium-ion battery, J. Power Sources, 448 (2020) 227425.
[10] Z. Liao, S. Zhang, Y. Zhao, Z. Qiu, K. Li, D. Han, G. Zhang, T.G. Habetler, Experimental evaluation of thermolysis-driven gas emissions from LiPF6-carbonate electrolyte used in lithium-ion batteries, Journal of Energy Chemistry, 49 (2020) 124-135.
[11] A. El Kharbachi, O. Zavorotynska, M. Latroche, F. Cuevas, V. Yartys, M. Fichtner, Exploits, advances and challenges benefiting beyond Li-ion battery technologies, Journal of Alloys and Compounds, 817 (2020) 153261.

[12] E.E. Ferg, F. Schuldt, J. Schmidt, The challenges of a Li-ion starter lighting and ignition battery: A review from cradle to grave, J. Power Sources, 423 (2019) 380-403.
[13] F.H. Gandoman, J. Jaguemont, S. Goutam, R. Gopalakrishnan, Y. Firouz, T. Kalogiannis, N. Omar, J. Van Mierlo, Concept of reliability and safety assessment of lithium-ion batteries in electric vehicles: Basics, progress, and challenges, Applied Energy, 251 (2019) 113343.
[14] Z.Y. Jiang, Z.G. Qu, J.F. Zhang, Z.H. Rao, Rapid prediction method for thermal runaway propagation in battery pack based on lumped thermal resistance network and electric circuit analogy, Applied Energy, 268 (2020) 115007.
[15] N. Zhang, H. Tang, Dissecting anode swelling in commercial lithium-ion batteries, J. Power Sources, 218 (2012) 52-55.
[16] F. Blanchard, B. Carré, F. Bonhomme, P. Biensan, D. Lemordant, Solubility of carbon dioxide in alkylcarbonates and lactones, Canadian Journal of Chemistry, 81 (2003) 385-391.
[17] G. Hong, J. Jacquemin, P. Husson, M.F. Costa Gomes, M. Deetlefs, M. Nieuwenhuyzen, O. Sheppard, C. Hardacre, Effect of Acetonitrile on the Solubility of Carbon Dioxide in 1-Ethyl-3-methylimidazolium Bis(trifluoromethylsulfonyl)amide, Industrial & Engineering Chemistry Research, 45 (2006) 8180-8188.
[18] Y.R. Dougassa, J. Jacquemin, L. El Ouatani, C. Tessier, M. Anouti, Low pressure methane solubility in lithium-ion batteries based solvents and electrolytes as a function of temperature. Measurement and prediction, Journal of Chemical Thermodynamics, 79 (2014) 49-60.
[19] Y.R. Dougassa, J. Jacquemin, L. El Ouatani, C. Tessier, M. Anouti, Viscosity and carbon dioxide solubility for LiPF6, LiTFSI, and LiFAP in alkyl carbonates: Lithium salt nature and concentration effect, Journal of Physical Chemistry B, 118 (2014) 3973-3980.
[20] Y.R. Dougassa, C. Tessier, L. El Ouatani, M. Anouti, J. Jacquemin, Low pressure carbon dioxide solubility in lithium-ion batteries based electrolytes as a function of temperature. Measurement and prediction, Journal of Chemical Thermodynamics, 61 (2013) 32-44.
[21] M. Anouti, Y.R. Dougassa, C. Tessier, L. El Ouatani, J. Jacquemin, Low pressure carbon dioxide solubility in pure electrolyte solvents for lithium-ion batteries as a function of temperature. Measurement and prediction, Journal of Chemical Thermodynamics, 50 (2012) 71-79.
[22] J. Xia, S.L. Glazier, R. Petibon, J.R. Dahn, Improving Linear Alkyl Carbonate Electrolytes with Electrolyte Additives, J. Electrochem. Soc., 164 (2017) A1239-A1250.
[23] L. Ma, J. Self, M. Nie, S. Glazier, D.Y. Wang, Y.-S. Lin, J.R. Dahn, A systematic study of some promising electrolyte additives in Li[Ni1/3Mn1/3Co1/3]O2/graphite, Li[Ni0.5Mn0.3Co0.2]/graphite and Li[Ni0.6Mn0.2Co0.2]/graphite pouch cells, J. Power Sources, 299 (2015) 130-138.
[24] N.N. Sinha, J.C. Burns, J.R. Dahn, Comparative Study of Tris(trimethylsilyl) Phosphate and Tris(trimethylsilyl) Phosphite as Electrolyte Additives for Li-Ion Cells, J. Electrochem. Soc., 161 (2014) A1084-A1089.

[25] J. Xia, R. Petibon, A. Xiao, W.M. Lamanna, J.R. Dahn, Some Fluorinated Carbonates as Electrolyte Additives for Li(Ni0.4Mn0.4Co0.2)O2/Graphite Pouch Cells, J. Electrochem. Soc., 163 (2016) A1637-A1645.
[26] Q.Q. Liu, D.J. Xiong, R. Petibon, C.Y. Du, J.R. Dahn, Gas Evolution during Unwanted Lithium Plating in Li-Ion Cells with EC-Based or EC-Free Electrolytes, J. Electrochem. Soc., 163 (2016) A3010-A3015.
[27] S. Komaba, M. Watanabe, H. Groult, N. Kumagai, Alkali carbonate-coated graphite electrode for lithium-ion batteries, Carbon, 46 (2008) 1184-1193.
[28] P. Verma, T. Sasaki, P. Novák, Chemical surface treatments for decreasing irreversible charge loss and preventing exfoliation of graphite in Li-ion batteries, Electrochimica Acta, 82 (2012) 233-242.
[29] J. Pires, L. Timperman, J. Jacquemin, A. Balducci, M. Anouti, Density, conductivity, viscosity, and excess properties of (pyrrolidinium nitrate-based Protic Ionic Liquid + propylene carbonate) binary mixture, Journal of Chemical Thermodynamics, 59 (2013) 10-19.
[30] C.M. Ghimbeu, C. Decaux, P. Brender, M. Dahbi, D. Lemordant, E. Raymundo-Pinero, M. Anouti, F. Beguin, C. Vix-Guterl, Influence of graphite characteristics on the electrochemical performance in alkylcarbonate LiTFSI electrolyte for Li-ion capacitors and Li-ion batteries, J. Electrochem. Soc., 160 (2013) A1907-A1915.
[31] S.-T. Myung, Y. Hitoshi, Y.-K. Sun, Electrochemical behavior and passivation of current collectors in lithium-ion batteries, Journal of Materials Chemistry, 21 (2011) 9891-9911.
[32] J. Kalhoff, D. Bresser, M. Bolloli, F. Alloin, J.-Y. Sanchez, S. Passerini, Enabling LiTFSI-based Electrolytes for Safer Lithium-Ion Batteries by Using Linear Fluorinated Carbonates as (Co)Solvent, ChemSusChem, 7 (2014) 2939-2946.
[33] J. Self, C.P. Aiken, R. Petibon, J.R. Dahn, Survey of Gas Expansion in Li-Ion NMC Pouch Cells, Journal of The Electrochemical Society, 162 (2015) A796-A802.
[34] F. Shaahmadi, B. Hashemi Shahraki, A. Farhadi, The CO2/CH4 gas mixture solubility in ionic liquids [Bmim][Ac], [Bmim][BF4] and their binary mixtures, The Journal of Chemical Thermodynamics, 141 (2020) 105922.
[35] C.A. Faúndez, E.N. Fierro, J.O. Valderrama, Solubility of hydrogen sulfide in ionic liquids for gas removal processes using artificial neural networks, Journal of Environmental Chemical Engineering, 4 (2016) 211-218.
[36] M.D. Ellegaard, J. Abildskov, J.P. O'Connell, Solubilities of gases in ionic liquids using a corresponding-states approach to Kirkwood-Buff solution theory, Fluid Phase Equilibria, 302 (2011) 93-102.
[37] J. Huang, A. Riisager, R.W. Berg, R. Fehrmann, Tuning ionic liquids for high gas solubility and reversible gas sorption, Journal of Molecular Catalysis A: Chemical, 279 (2008) 170-176.

[38] M. Hilder, G.M.A. Girard, K. Whitbread, S. Zavorine, M. Moser, D. Nucciarone, M. Forsyth, D.R. MacFarlane, P.C. Howlett, Physicochemical characterization of a new family of small alkyl phosphonium imide ionic liquids, Electrochimica Acta, 202 (2016) 100-109.
[39] K. Tsunashima, Y. Ono, M. Sugiya, Physical and electrochemical characterization of ionic liquids based on quaternary phosphonium cations containing a carbon–carbon double bond, Electrochimica Acta, 56 (2011) 4351-4355.
[40] K. Tsunashima, A. Kawabata, M. Matsumiya, S. Kodama, R. Enomoto, M. Sugiya, Y. Kunugi, Low viscous and highly conductive phosphonium ionic liquids based on bis(fluorosulfonyl)amide anion as potential electrolytes, Electrochemistry Communications, 13 (2011) 178-181.
[41] P. Kolář, H. Nakata, J.W. Shen, A. Tsuboi, H. Suzuki, M. Ue, Prediction of gas solubility in battery formulations, Fluid Phase Equilibria, 228-229 (2005) 59-66.

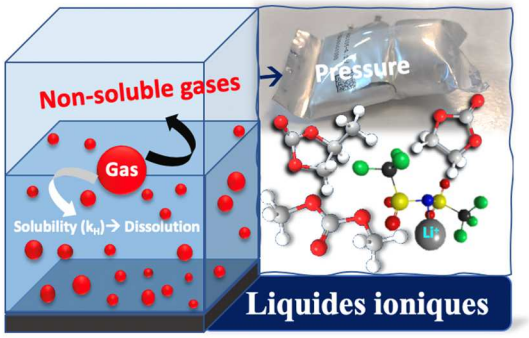
Non-soluble gases
Gas
Solubility ($k_H$)→ Dissolution
Pressure
Li+
Liquides ioniques